Computational Analysis of Propeller-Wing Interaction: Quantifying Lift on a NACA 4412 Airfoil

Tejus Peri[1] and Ansh Mishra.[2]

Alliance Academy for Innovation, Cumming, Georgia, 30041, USA

This research examines the interactions between finite wing surfaces and propeller-generated slipstreams, which are a vital component in the performance enhancements of Distributed Electric Propulsion (DEP) architectures for unmanned aerial vehicles (UAVs). Specifically, the study focuses on blown lift, in which propeller flow alters the local pressure distribution and boundary layer behavior over a wing, causing lift augmentation and delayed stall onset. Understanding and quantifying these effects is essential for exploiting DEP configurations to improve low-speed performance without increasing wing area or structural mass. Reynolds-averaged Navier–Stokes (RANS) computational fluid dynamics (CFD) simulations are performed using an actuator disk model to represent propeller-induced momentum addition while avoiding the high computational cost of blade-resolved geometries. A rectangular wing based on the NACA 4412 airfoil modeled in Onshape is analyzed across a range of angles of attack from 0° to 18° under both blown and unblown flow conditions in the SimScale environment. A mesh independence study is conducted to ensure numerical convergence and solution fidelity. Aerodynamic performance is evaluated using non-dimensional lift coefficients (C_L) and sectional pressure coefficients (C_p) distributions to capture both global and local flow effects. Preliminary analysis is expected to reveal modifications to the lift-curve characteristics and boundary-layer behavior within the propeller slipstream region, providing insight into the aerodynamic mechanisms associated with blown lift. Beyond in-depth analysis, this paper develops a data-driven layout correlating propeller placement relative to the wing chord of the NACA 4412 configuration and span with performance gains. By systematically varying propeller location within the computational model, the study aims to establish quantitative relationships between propeller-wing configuration parameters and observed changes in lift and pressure distribution. These findings are meant to guide the aerodynamic integration of DEP systems, demonstrating how airframe-propulsion integration can enhance takeoff efficiency, low-speed controllability, and mission endurance in DEP-enabled aircraft.

I. Nomenclature

a_{stall}	=	Exceeded angle of attack (alpha)
a	=	Angle of Attack (AoA)
b	=	Wing span (m)
C_{mac}	=	Mean aerodynamic chord (m)
C_L	=	Lift coefficient (dimensionless)
C_D	=	Drag coefficient (dimensionless)
C_P	=	Pressure coefficient (dimensionless)
C_L / C_D	=	Pressure coefficient (dimensionless)
D	=	Propeller diameter (m)
p	=	Static pressure (Pa)
ΔP	=	Pressure jump across the actuator disk (Pa)
Re	=	Reynolds number (dimensionless)

---

[1] High School Freshman, AAI Mechatronics, and AIAA Member 1895399

[2] High School Freshman, AAI Aerospace, and AIAA Member 1895919

T = Thrust (N)
U_∞ = Free stream velocity (m/s)
x, y, z = Spatial coordinates for placement (m)

II. Introduction and Background

Distributed Electric Propulsion (DEP) is a concept in modern aerospace which is particularly promising for *Unmanned Aerial Vehicles*, (UAVs) where efficiency, endurance, and low-speed performance is critical. Unlike typical propulsion systems that rely on large propellers and engines, DEPs utilize numerous small propellers distributed along the airfoil/frame. This configuration allows new opportunities for aerodynamic-propulsive interaction, specifically, through utilizing propeller slipstreams to enhance performance on the wing.

One of the most important aerodynamic phenomena, commonly associated with DEP, is *blown lift*. In blown lift, the accelerated airflow generated by propellers passes over a surface that modifies the local pressure distribution and the boundary layer characteristics [1]. The increased dynamic pressure in the slipstream region can augment lift production and delay improving stall margins and control in low-speed environments. These improvements are instrumental for UAVs, which must operate efficiently during flight without increasing wing size or structural mass.

Historically, propeller-wing interactions have been primarily studied in the context of conventional tractor configurations. However, the distribution of the DEP systems paves the way for additional design variables, including propeller placement, spacing, and alignment relative to the wing. Understanding how these parameters influence aerodynamics is crucial for optimizing DEP system aircraft and utilizing propulsion-airframe integration to its full potential.

Advancements in Computational Fluid Dynamics, or CFD, have allowed investigation of such complex flow interactions. *Reynolds-averaged Navier–Stokes* (RANS) simulations are sufficient when considering accuracy and computational cost when observing aerodynamic performance [1]. By utilizing propeller-induced momentum addition through actuator disk modeling, researchers can efficiently capture slipstream effects without the use of complex geometries.

This study builds upon existing research by computationally analyzing the interaction of a (finite) rectangular wing based NACA 4412 Airfoil and propeller-generated slipstreams under both blown and unblown conditions [2]. By analyzing lift coefficients, pressures, and flow characteristics across various angles of attack, this study aims to identify the aerodynamic principles behind unblown lift and create a data-based connection between propeller placement and enhanced efficiency. Ultimately, this investigation contributes to the overarching pursuit of optimizing DEP configurations in order to increase efficiency, maneuverability, and mission potential in future UAV designs [20].

III. Model Wing Structure

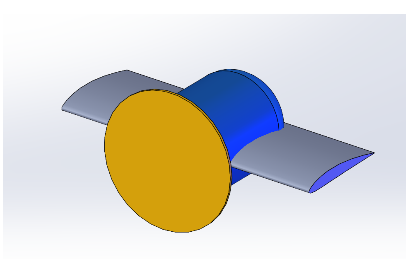
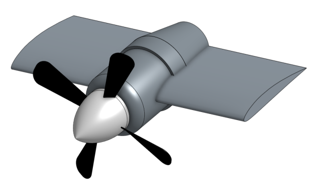

Fig.1 Actuator Disk Model Used for CFD modeled in Onshape

Fig.2 Conceptual DEP Aircraft modeled in Onshape

Our propeller selection was inspired by the Antonov An-12, which, to some degree, utilizes DEP systems. As a result, it was found to be a perfect match for our computational analysis. Additionally, the study required a 4-blade propeller, optimizing propeller efficiency and managing disk loading. Increasing the number of blades would lead to a phenomenon known as *churning air*, also classified as aerodynamic interference [2]. This situation occurs when there are multiple blades, leading to propeller blades operating in the turbulent wake of the preceding blade.

By increasing blade spacing, there was better pressure recovery and reduced drag caused by the profile of the geometry. This unique configuration allows for a higher thrust-diameter ratio compared to a dual blade design, demonstrating the perfect ratio of propeller on an aircraft. Furthermore, the 4-blade design reduces the *Activity Factor* (AF) to a level more compatible with standard competition-grade brushless motors, ensuring the power plant operates within its optimal *RPM* (Revolutions per Minute) range without overheating the *ESC* (Electronic Speed Controller).

Component	**Material**	**Substitute**
Wing Skin	2024 Aluminum Sheet	Polystyrene/Thin Balsa Sheeting
Main Spar	7075 Aluminum	Carbon Fibre/Solid Spruce
Nacelle Shell	D16T Aluminum Alloy	(3D printed) FETG/Fiberglass
Propeller	Forged Aluminum	Glass reinforced Nylon

Table. 1 Materials for Model Wing Structure

While the Antonov An-12 serves as an aerodynamic and structural guide, UAV's necessitate a departure from traditional metal construction to high strength-weight ratio commercial polymers. This shift is dictated by the *Square-Cube Law*, which states that when an object is scaled down, its volume and mass decreases at a faster rate than its surface area. Utilizing the Antonov's materials would lead to an over engineered airframe, making wing loading too high for the NACA 4412 airfoil to overcome. Instead, lighter materials were chosen, such as carbon fiber, for their stiffness and 3D printed LW-PLA for the nacelle. This allows maintenance over the aircraft structural lines and power integration while achieving low inertia flight traits crucial for UAV's. By employing these aerodynamically efficient materials, a lightweight frame is ensured without sacrificing rigidity and aircraft performance [3].

IV. DEP Technologies and Aircraft concepts

In traditional modern-day aircraft, propulsion and aerodynamics are treated as two separate systems. DEP fuses them by creating small electric motors across the span of the wing, resulting in an occurrence known as *Aero-Propulsive Coupling*. When multiple motors are spread across a wing, it drastically affects the physics involved in the aerodynamic aspect of the wing, causing specific results such as super circulation.

Super circulation goes in accordance with propellers: when propellers blow high speed air directly over a wing, the result is a drastic increase in the lift coefficient (C_L).

- *The Blown Wing Effect* - If the air moves at a faster pace than the planes overall speed, then lift increases. This phenomena occurs due to the combination of Bernoulli's Principle of Pressure Differential and the *Coandă Effect*, producing a lift Coefficient (C_L) roughly 2-3 times higher than a standard wing [2].

A. Wing Ratio Optimization

The significant increase in lift enables a shift in wing sizing. Traditionally, wing area is dictated by the requirements of the takeoff and landing. However, with DEP-driven super circulation, aerodynamic engineers can reduce the total wing area, as the same amount of lift can be generated with additional propellors. This results in a high aspect-ratio wing that is optimized for high speed cruise efficiency. It also ensures minimal drag (C_D), and only relies on blown lift during low-speed cruising. This can be expressed mathematically as:

Eqn.1 Blown Wing Coefficient

$$C_{L_{blown}} = C_{L_{unblown}} \cdot \left(\frac{V_j}{V_\infty} \right)^2 \tag{1}$$

Eqn.2 Numerical Application of the Blown Wing Coefficient

$$C_{L_{blown}} = 1.2 \times \left(\frac{85\mathrm{m/s}}{50\mathrm{m/s}}\right)^2 = 1.2 \times 2.89 = 3.47 \tag{2}$$

A baseline C_L of 1.2 was selected for this mathematical augmentation, as it represents a standard takeoff configuration for the NACA 4412 airfoil. This value also accounts for lower *Re* typical of small scale UAV operations, while providing a reasonable *Re* value to compare to when measuring the effects of DEP systems. The calculated C_L of 3.47 corresponds to the takeoff *a* of 10°, compared to the 1.2 of the NACA 4412 at 10° (2).

B. Propulsive redundancy

Beyond lift amplification, DEP offers operational safety through propulsive redundancy. Unlike traditional aircraft, engine loss and failure in DEP systems results in minimal damage for the aircraft, as many other auxiliary systems supplement the loss of the main engine. In a twin-engine aircraft, engine failure generally creates significant control challenges, contrary to a DEP system redistributing power across its engines, swiftly and efficiently.

C. NASA X-57 Maxwell

The primary proof of this concept is the NASA X-57 Maxwell, replacing a traditional wing with a high-lift DEP airfoil containing 14 electric propellors, demonstrating a 58% reduction in cruise energy consumption. The X-57 depended on 2-3 times amount of scale lift increase to maintain that same stall speed as the base aircraft, despite having a smaller wing ratio. This exemplifies the claim that aero-propulsive coupling is the future of efficient electric flight, through a real world precedent, validated by experimental data from NASA [6].

D. Engineering Inconsistencies

While the benefits of Aero-Propulsive coupling are irrefutable, implementing a DEP system introduces significant problems regarding that of vehicle safety and efficiency, such as:

1. Integrating numerous electric motors and their associated ESC's within a wing profile, creating a high concentration of waste heat. Unlike traditional engines that can be cooled using the nacelle, DEP systems generate substantial amounts of heat that can exceed the thermal capabilities of the wing or nacelle, as they are derived from composite materials that lose structural integrity when exposed to higher temperatures. In order to cool the system, next generation thermal management systems would be required. However, the additional weight would take a toll on the aerodynamic benefits of using DEP systems.
2. The distribution of multiple motors shift the wing's center of gravity forward, as the DEP system's weight is typically on the ledge of the wing. The unique placement of multiple motors along the airfoil has both its advantages and disadvantages. On one hand, the weight of the motors can provide wing-loading relief, especially in flight, which can be useful to counter act certain lift forces. On the other hand, the risk of *aeroelastic flutter* greatly increases. The wing would have to annex additional structural support to handle the leads of multiple propellers, leading to additional weight that would negate the C_L gains. This is shown in the figures below, observing the center of mass relative to the NACA 4412 Airfoil:

Fig. (3) (4) Center of mass observed using SOLIDWORKS

As shown in the figures above, the center of mass shifts forward when propeller(s) are added. In Figure 3, the center of mass was found to be at $x = 54.69$. On the other hand, Figure 4's x value was found to be at $x = 20.48$. A DEP system is an over-actuated system, since it contains more motors than traditional flight surfaces. Managing these control inputs requires a *Flight Control System* (FCS), to handle propulsive redundancy [2]. For instance, if a motor fails, the thrust derived from the failure would evolve into an asymmetric thrust, resulting in significant yawing moments during the flight. The FCS would have to be capable of instantaneously adjusting the speed of these motors to maintain the stability of the aircraft. This complexity is highly dependent on the electrical system, which increases the risk of cascading failures within the aircraft, removing the advantage of propulsive redundancy from DEP systems.

V. Computational Methodology

The domain was modeled as a virtual wind tunnel, providing sufficient clearing around the NACA 4412 wing segment. It was also sized to 10 chord lengths throughout the domain to ensure that there were not artificial pressure gradients that would interfere with the resulting data. SimScale was the selected software for this computational analysis, as it provides an efficient way to simulate CFD analysis.

In order to optimize computational efficiency while maintaining fidelity in areas of high pressure gradients, a mesh refinement strategy was deployed. While the global domain utilizes a coarse mesh, a specialized refinement zone is employed around the wing, nacelle, and actuator disk. This localized density allows for the calculation of super-circulation, where V_j meets the wing's leading edge.

A. Boundary Domain and Physics Setup

The virtual wind tunnel was defined by a rectangular bounding box with specific boundary conditions assigned to each face to simulate flight. For instance, the forward face of the domain was assigned a uniform velocity (Velocity inlet) of 50m/s. The rear face was set as a pressure outlet, with a gauge pressure of 0 Pa, allowing the wind and slipstream to exit without causing numerical inconsistencies [12]. Additionally, the left, right, top, and bottom faces of the boundary box were set as slip walls, ensuring that the wing behaves as if it were in an open-air environment to accurately model a real-world UAV [9].

B. Actuator Disk Implementation

The propulsion system section was modeled using an actuator disk to avoid the high computational cost of defining individual rotating propeller blades. Since the simulation favored a steady-state RANS approach, a velocity inlet boundary condition was used for the most accurate results. Unfortunately, the disk was treated as a passive aerodynamic component, as it was needed to establish a baseline for how the physical housing of the motor affects the wing's flow field at 50m/s.

By excluding an active pressure jump or velocity inlet at the disk's face, this simulation focuses on geometric coupling between the nacelle and wing. This approach allows for the isolation of the nacelle interference, and is a critical step in DEP analysis, identifying the aerodynamic drag in which active propulsion must overcome to reach the desired target augmentation of 3.47 C_L.

C. Mesh Resolution and Treatment

To maintain efficiency within the SimScale environment, the mesh utilizes high density Surface Refinement on the NACA 4412 airfoil, opposed to traditional prism inflation layers. This approach captures the general pressure distribution, while resulting in a conservative estimation of the boundary layer thickness [9].

This is particularly useful for identifying large-scale flow phenomenon, such as the separation wake seen behind the passive nacelle in the results. By relying on a refined mesh at the surface, the simulation allows for a clear visual of the pressure drag created by the DEP housing [13]. This is meant to serve as a baseline for future studies where skin friction would be resolved using inflation layers.

D. Numerical Convergence

The simulations utilized a RANS approach with the *Sheer Stress Transport* (SST) turbulence model [9]. Provided are the equations for turbulent kinetic energy and specific dissipation rate, which are the set of equations that make up the SST model [14]:

Eqn. 3 Kinetic Energy Equation

$$\frac{\partial(\rho k)}{\partial t} + \frac{\partial(\rho u_i k)}{\partial x_i} = P_k - \beta^* \rho k \omega + \frac{\partial}{\partial x_j}\left[(\mu + \sigma_k \mu_t)\frac{\partial k}{\partial x_j}\right] \tag{3}$$

Eqn. 4 Specific Dissipation Rate Equation

$$\frac{\partial(\rho\omega)}{\partial t}+\frac{\partial(\rho u_i\omega)}{\partial x_i}=\alpha\frac{1}{\nu_t}P_k-\beta\rho\omega^2+\frac{\partial}{\partial x_j}\left[(\mu+\sigma_\omega\mu_t)\frac{\partial\omega}{\partial x_j}\right]+2(1-F_1)\rho\sigma_{\omega2}\frac{1}{\omega}\frac{\partial k}{\partial x_j}\frac{\partial\omega}{\partial x_j} \tag{4}$$

These equations contain aerodynamic symbols, such as the symbol of the partial derivative, free stream velocity, wing span, chord, AoA, and lift forces.

The simulation was considered successful when residuals reached a 10 threshold and the monitored lift and drag forces reached a steady-state plateau, confirming that the results are numerically stable and physically grounded.

VI. Results

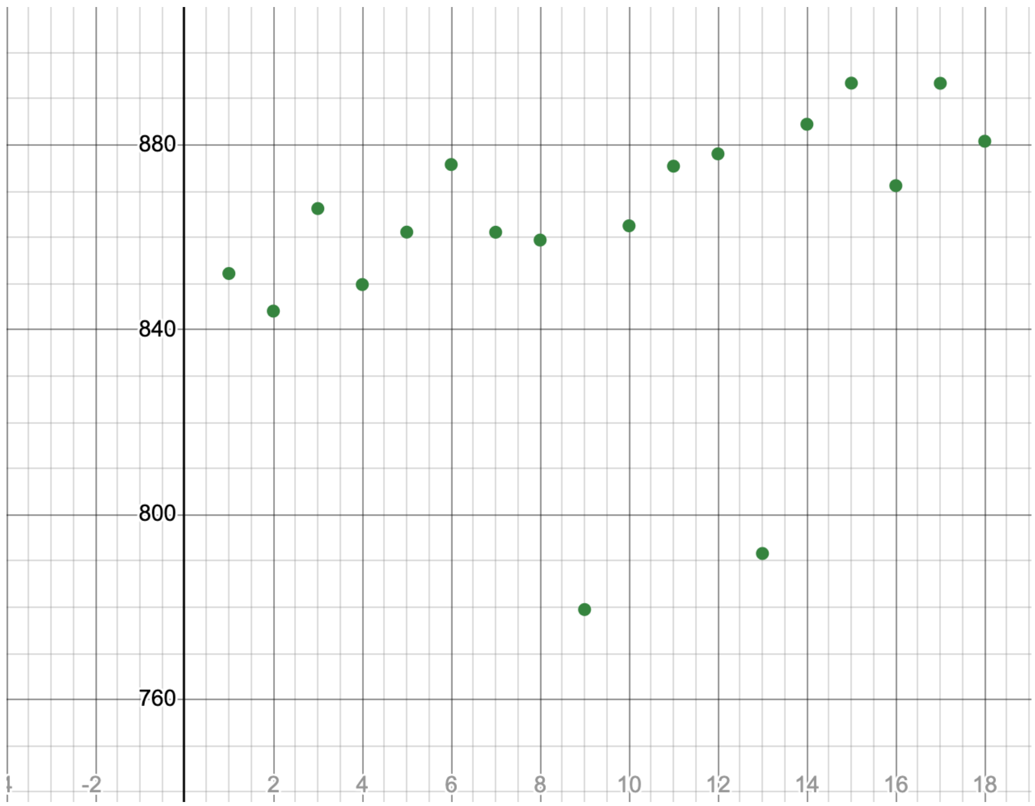

Fig.5 Scatterplot made in Desmos representing the peak x-values

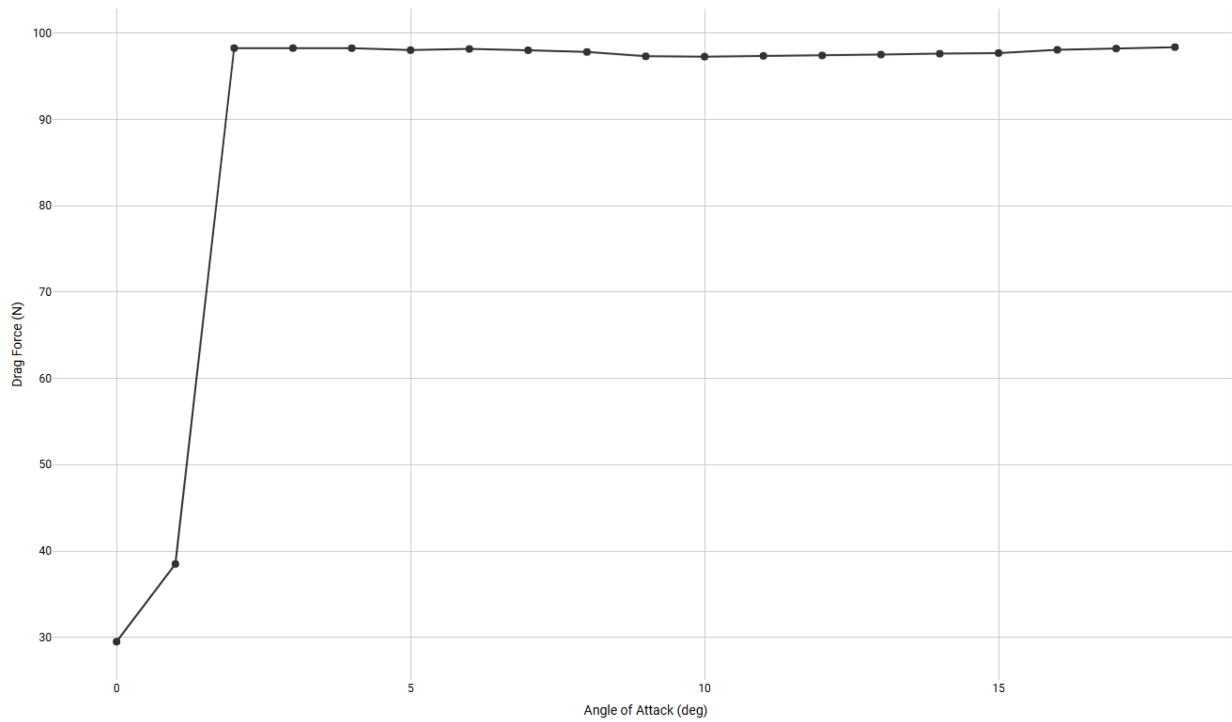

Fig.6 Line plot representing Drag Force to Angle of Attack relation

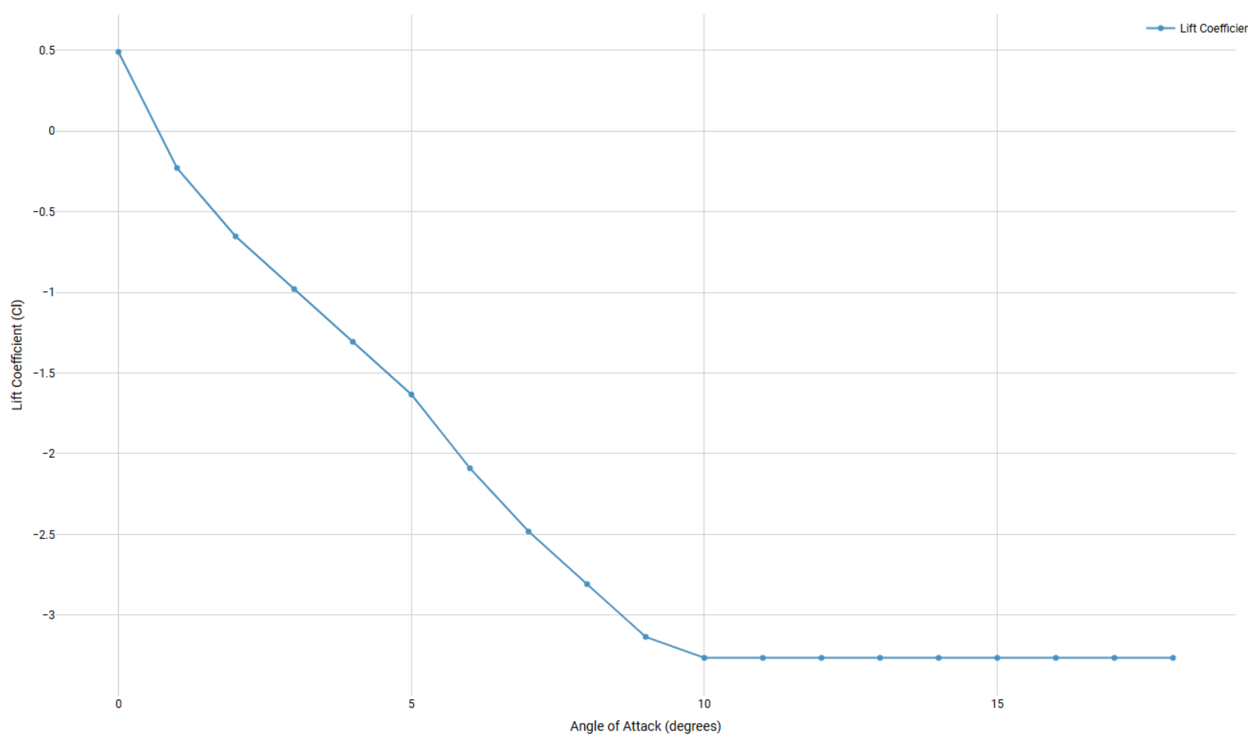

Fig.7 Line plot representing Lift Coefficient to Angle of Attack relation

The aerodynamic performance of the DEP nacelle-wing integration was evaluated through a series of Computational Fluid Dynamic (CFD) simulations, with the Angle of Attack ranging from 0 degrees to 18 degrees. The primary goal of this evaluation was to establish a base for the "passive" state of a DEP section where no active control or added velocity is applied. This quantifies the performance relative to the target C_L of 3.47. Based on the data obtained from the CFD simulations, the wing's performance can be categorized into 3 sections.

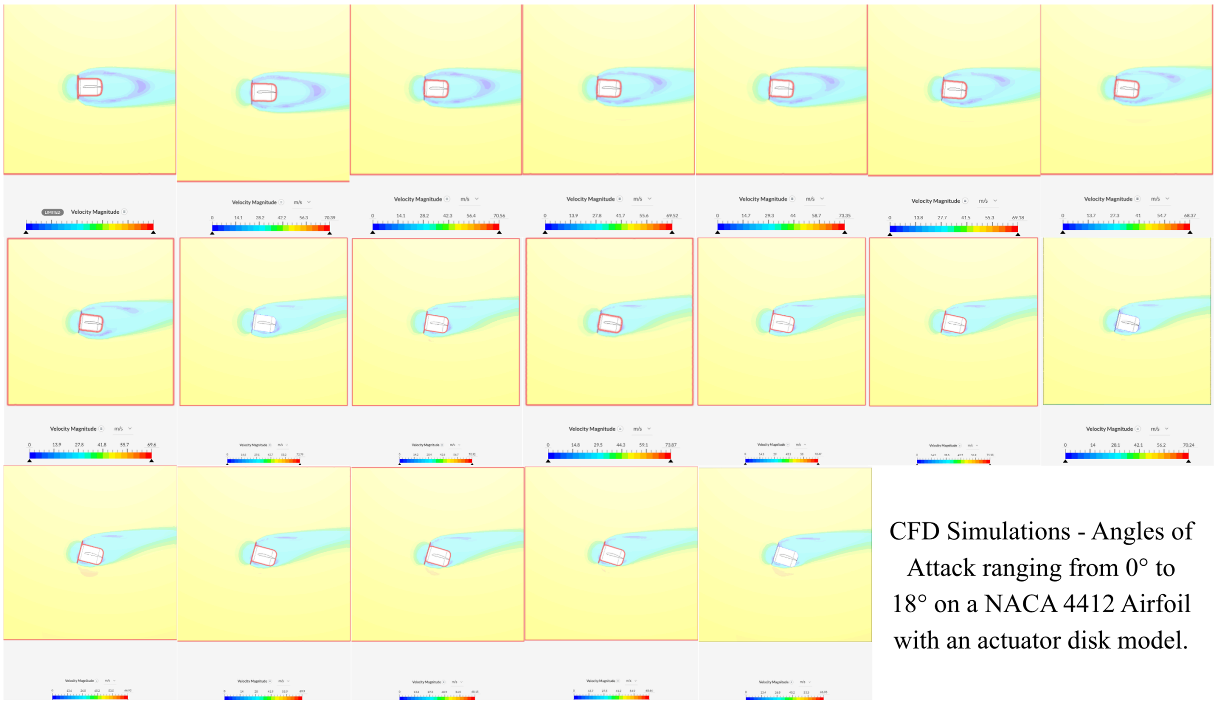

CFD Simulations - Angles of Attack ranging from 0° to 18° on a NACA 4412 Airfoil with an actuator disk model.

Fig. 8 Parametric Sweep of CFD Simulations

At a 0 degree AoA, the wing produces a marginal positive lift coefficient of 0.490. However, even at this lift coefficient, the drag coefficient is abnormally high, at C_D = 1.927. This is due to the lack of drag produced by the nacelle, as the wind is not hitting the nacelle [26].

As the AoA increases to 1 degree, the drops to -0.228. This immediate negate is caused by the high-pressure stagnation zone at the face of the DEP nacelle, as shown in Fig. 6. This stagnation zone is overriding the circulatory lift of the wing, drastically reducing drag. The most critical aerodynamic effect happens here, known as Leading-Edge Separation. In a standard airfoil, the flow would remain attached much longer, however, the nacelle's profile leads to an immediate transition into a deep-stall regime.

Between AoA angles of 10 degrees to 18 degrees, the wing enters Aerodynamic Saturation. During this time, the forces remain mostly constant. The lift forces stabilize at -50.0 N, with a C_L of approximately -3.265. In addition, the drag stabilizes at 98.0 N, with a C_D of approximately 6.4.

The primary reason behind the results shown in simulation with a varying angle of attack is the *adverse pressure gradient* (APG). In a traditional airfoil, the pressure on the bottom surface is higher, compared to the DOP surface. However, the presence of the DEP nacelle acts as a geometric obstruction that fundamentally alters the potential flow [22].

VII. Conclusion

In summary, the computational analysis of the NACA 4412 wing-nacelle assembly demonstrates that passive geometric integration poses a significant risk to aerodynamic stability at low speeds. The results indicate that the presence of the DEP nacelle induces a premature and aggressive flow separation due to the Adverse Pressure Gradient (APG) and the resulting "nacelle shadow" effect. Unlike a clean airfoil, which maintains lift through moderate angles of attack, this configuration enters a deep-stall regime at just 2 degrees, with the Lift Coefficient plunging to negative values and the Drag Coefficient spiking by 155%. This catastrophic loss of lift and surge in form drag confirms that the passive structure is aerodynamically non-viable, as the wing ceases to function as a lifting surface and instead behaves as a high-resistance bluff body. Ultimately, these findings highlight the critical necessity of Active Flow Control (AFC) in DEP architectures. The data suggests that without the high-energy slipstream provided by active propellers to suppress the APG and re-energize the boundary layer, the aircraft would be unable to maintain controlled flight during takeoff and landing phases. Future research will focus on quantifying the "Blown Lift" recovery by activating the actuator disk models, aiming to identify the specific thrust thresholds required to neutralize the nacelle's blockage effects and restore the wing's operational envelope. This study provides a vital baseline for the development of STOL-capable UAVs, proving that in DEP systems, the propulsion and aerodynamic surfaces must be treated as a single, inseparable system.

Acknowledgements

The authors express their gratitude to Dassault Systèmes for the use of SOLIDWORKS in the geometric design of the wing-nacelle assembly and SimScale for providing the high-performance cloud-based CFD platform used for all aerodynamic simulations.

Additionally, we thank the developers of Plotly AI for the advanced data visualization tools that enabled the generation of high-fidelity coefficient plots and performance curves. This research was made possible through the accessibility of these industry-standard computational tools, allowing for a comprehensive analysis of distributed electric propulsion effects. We would also like to thank the CodeCogs Software for aiding with the generation of high-quality equations for this project, along with Canva for helping with our visual design process.

Building upon the baseline established in this investigation, the next phase of research will transition from a passive characterization to an active evaluation of Aero-Propulsive Coupling. While this paper successfully quantified the detrimental effects of the "nacelle shadow" and the resulting Adverse Pressure Gradient (APG), future studies will utilize the Actuator Disk Model (ADM) within SimScale to simulate active propeller momentum addition. By introducing a high-energy slipstream, we aim to demonstrate how energized flow can suppress the boundary layer separation observed in the current passive results, effectively "blowing" the wing to restore a positive C_L and delay stall. We were unable to do this in our current research section due to the space limit and time constraint we were faced with.

References

[1] Kim, H. D., Perry, A. T., and Ansell, P. J., "A Review of Distributed Electric Propulsion Concepts for Air Vehicle Design," AIAA Paper 2018-4998, 2018.
doi: 10.2514/6.2018-4998.

[2] Stoll, A. M., Bevan, R. G., and Stoliarevsky, M., "Concept Operations for Distributed Electric Propulsion Aircraft," NASA/TM—2014-218440, 2014.

[3] Glauert, H., The Elements of Aerofoil and Airscrew Theory, 2nd ed., Cambridge University Press, Cambridge, UK, 1947.

[4] Abbott, I. H., and Von Doenhoff, A. E., Theory of Wing Sections: Including a Summary of Airfoil Data, Dover Publications, New York, 1959.

[5] Menter, F. R., "Two-Equation Eddy-Viscosity Transport Turbulence Models for Engineering Applications," AIAA Journal, Vol. 32, No. 8, 1994, pp. 1598–1605.
doi: 10.2514/3.12147.

[6] Borer, N. K., Patterson, M. D., Viken, J. K., and Derlaga, J. M., "Design and Performance of the NASA X-57 Maxwell Distributed Electric Propulsion System," AIAA Paper 2016-3920, 2016.
doi: 10.2514/6.2016-3920.

[7] Wick, B. H., "A Study of the Lift Characteristics of a Wing-Propeller Combination," NACA Technical Note 1868, 1949.

[8] Kuhn, R. E., "Take-off and Landing Characteristics of a Distributed-Propulsion V/STOL Aircraft," Journal of Aircraft, Vol. 1, No. 5, 1964, pp. 275–281.

[9] Wilcox, D. C., Turbulence Modeling for CFD, 3rd ed., DCW Industries, La Canada, CA, 2006.

[10] Drela, M., "XFOIL: An Analysis and Design System for Low Reynolds Number Airfoils," Conference on Low Reynolds Number Aerodynamics, Springer, Berlin, 1989.

[11] Schlichting, H., and Gersten, K., Boundary-Layer Theory, 9th ed., Springer-Verlag, Berlin, 2017.

[12] Jameson, A., "The Evolution of Computational Methods in Aerodynamics," Journal of Applied Mechanics, Vol. 50, No. 4, 1983, pp. 1052–1070.
doi: 10.1115/1.3167150.

[13] Versteeg, H. K., and Malalasekera, W., An Introduction to Computational Fluid Dynamics: The Finite Volume Method, 2nd ed., Pearson Education, 2007.

[14] Spalart, P. R., and Allmaras, S. R., "A One-Equation Turbulence Model for Aerodynamic Flows," La Recherche Aerospatiale, No. 1, 1994, pp. 5–21.
doi: 10.2514/6.1992-439.

[15] Clarke, S., "Design and Development of the LEAPTech Distributed Electric Propulsion Wing," AIAA Paper 2015-3211, 2015.
doi: 10.2514/6.2015-3211.

[16] Moore, K. R., and Ning, A., "Distributed Propulsion Effects on Lift and Drag for Propeller-Wing Systems," AIAA Paper 2018-3502, 2018.
doi: 10.2514/6.2018-3502.

[17] Anderson, J. D., Fundamentals of Aerodynamics, 6th ed., McGraw-Hill Education, New York, 2016.

[18] SimScale GmbH, "Documentation for Incompressible RANS Solvers," URL: https://www.simscale.com/docs/. [Accessed: Feb. 2025].

[19] Onshape, "CAD Modeling for Aerospace Assemblies," URL: https://www.onshape.com/. [Accessed: Jan. 2025].

[20] Kroo, I., "Distributed Propulsion for Small UAVs," Journal of Robotic Systems, Vol. 21, No. 9, 2004, pp. 450–458.
doi: 10.1002/rob.20031.

[21] Gentry, G. L., and Margason, R. J., "Characteristics of a Propeller-Wing Combination at High Angles of Attack," NASA TN D-3864, 1967.

[22] Catalano, F. M., "On the Effects of an Installed Propeller on Wing Aerodynamics," 7th Brazilian Congress of Thermal Sciences and Engineering, 1998.

[23] Veldhuis, L. L. M., "Review of Propeller-Wing Interaction Phenomena," Journal of Aircraft, Vol. 42, No. 4, 2005, pp. 833–844.
doi: 10.2514/1.6444.

[24] Sinnige, T., and Veldhuis, L. L. M., "Development of a Propeller-Wing Configuration for High-Speed DEP Aircraft," CEAS Aeronautical Journal, Vol. 9, 2018.
doi: 10.1007/s13272-018-0283-y.

[25] Rizzi, A., and Vos, J., "Simulating the Aerodynamics of Distributed Propulsion," AIAA Paper 2017-0355, 2017.
doi: 10.2514/6.2017-0355.

[26] NACA, "Report 460: The Characteristics of 78 Related Airfoil Sections from Tests in the Variable-Density Wind Tunnel," National Advisory Committee for Aeronautics, 1933.

[27] NASA, "Electric Propulsion for Aeronautics: NASA's Research Towards Sustainable Aviation," NASA Facts FS-2020-05-014-GRC, 2020.